Spatiotemporal and Higher-Order Instabilities in Kerr Optical Frequency Combs

AURÉLIEN COILLET[1,2], ZHEN QI[3], IRINA V. BALAKIREVA[1], GUOPING LIN[1,4], CURTIS R. MENYUK[3,*], AND YANNE K. CHEMBO[1,5,†]

[1] *FEMTO-ST Institute, Univ. Bourgogne Franche-Comté, CNRS, Optics Department, 15B Avenue des Montboucons, 25030 Besançon cedex, France*
[2] *Institut Carnot Bourgogne, Univ. Bourgogne-Franche-Comté, 9 Avenue A. Savary, 21078 Dijon, France*
[3] *Department of Computer Science and Electrical Engineering, University of Maryland Baltimore County, 1000 Hilltop Circle, Baltimore, Maryland 21250, USA*
[4] *MOE Key Laboratory of Fundamental Quantities Measurement, School of Physics, Huazhong University of Science and Technology, Wuhan 430074, China*
[5] *Institute for Research in Electronics and Applied Physics (IREAP), & Department of Electrical and Computer Engineering, University of Maryland, College Park MD 20742, USA.*
[*] *menyuk@umbc.edu*
[†] *ykchembo@umd.edu*

Compiled February 11, 2019

We demonstrate that extended dissipative structures in Kerr-nonlinear whispering-gallery mode resonators undergo a spatiotemporal instability as the pumping parameters are varied. The dynamics of the patterns beyond this bifurcation yield specific Kerr comb and sub-comb spectra that can be subjected to phase of frequency-locking when optimal conditions are met. We also report for the first time the existence of fourth-order combs, which can be excited instead of the conventional secondary combs when roll patterns loose their stability.

OCIS codes: To be updated later.

http://dx.doi.org/10.1364/optica.XX.XXXXXX

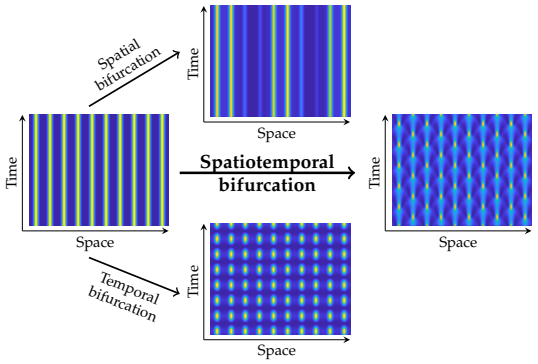

Fig. 1. Illustration of a spatiotemporal bifurcation for the rolls in the LLE. A stable set of Turing rolls could in principle undergo several types of bifurcations: a spatial bifurcation will lead to a spatially modulated pattern, while a temporal bifurcation will produce oscillations along the time coordinate. In contrast, a spatiotemporal bifurcation leads to patterns that oscillate both in time and space.

Spatiotemporal instabilities arise when a stationary solution looses stability via a traveling wave. Although well-known in the context of the mathematical analysis of nonlinear partial differential equations, unambiguous examples of such instabilities are not very common in nonlinear optics. Noteworthy exceptions include ref. [1], where the authors analyzed spatiotemporal instability of a constant field (flat state) in a nonlinear medium with both dispersion and diffraction. More recently, Anderson *et al.* reported in ref. [2] investigated theoretically and experimentally the spatiotemporal instability from a temporal cavity soliton in a fiber ring resonator.

In this letter, we show that the Turing rolls in Kerr-nonlinear whispering-gallery mode (WGM) resonators loose their stability via such spatiotemporal instabilities. This bifurcation also provides an explanation related to some of the unexplained phase-locking phenomena that have been reported in recent experimental works.

The system under investigation is an ultra-high Q WGM resonator pumped by a resonant continuous-wave laser. The dynamics of the normalized intracavity field $\psi(\theta,\tau)$ obeys the

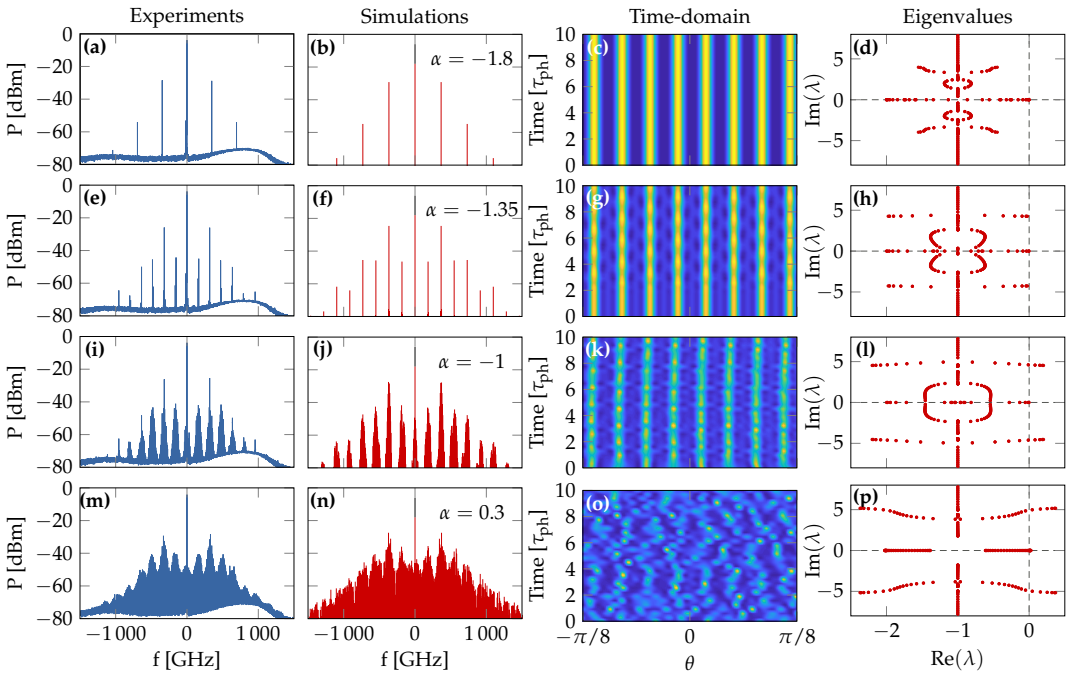

Fig. 2. Experimental transition to secondary combs and chaos obtained with a MgF_2 resonator by detuning the laser further into resonance ($\alpha = -1.8, -1.35, -1$ and 0.3) with constant pump power $F^2 = 12$. The FSR of the resonator is ~ 5.9 GHz, its intrinsic and coupling quality factors are $\sim 10^9$ at 1550 nm, corresponding to a photon lifetime $\tau_{ph} = 0.8\ \mu$s. Corresponding simulations spectra and time-domain evolution are shown in the second and third column. The last column displays the eigenvalues in the complex plane: the spatiotemporal bifurcation occurs when the real part of one of them becomes positive, close to the detuning $\alpha = -1.35$.

following Lugiato-Lefever Equation (LLE) [3–5]

$$\frac{\partial \psi}{\partial \tau} = -(1 + i\alpha)\psi + i|\psi|^2\psi - i\frac{\beta}{2}\frac{\partial^2 \psi}{\partial \theta^2} + F\,, \qquad (1)$$

where the normalized parameters are the laser-cavity detuning α, the second-order dispersion β, and the pump field F, while the variables are the dimensionless time τ and the azimuthal angle $\theta \in [\pi, \pi]$. This equation does not account for the other third-order nonlinearities of the bulk resonator, that could trigger instabilities of their own [6, 7].

The most prevalent extended dissipative structures in the cavity are the so-called Turing roll patterns. These patterns emerge from a flat state via a Turing instability, and are constituted by an integer number of rolls along the azimuthal direction of the resonator. Previous theoretical analysis have shown that at threshold, this number is the closest integer approximation of $L_{th} = [2(\alpha - 2)/\beta]^{\frac{1}{2}}$. The Kerr comb spectra corresponding to this roll patterns are sometimes referred to as primary combs, and they feature multiple-FSR spacing, with a multiplicity exactly equal to L_{th} [8–10]. An open point is to understand how these rolls loose their stability, as the pump parameters (power and frequency) are varied. Figure 1 proposes a schematic illustration of the possible destabilization mechanisms for a roll pattern, that include temporal spatial, and spatiotemporal bifurcations. Our main objective in this letter is to show that it is the latter that rules the destabilization of azimuthal roll patterns in WGM resonators. The stationary solutions of the LLE satisfy Eq. (1) with $\partial_\tau \psi \equiv 0$. Once a steady- state solution ψ_{st} has been found, its stability may be determined by linearizing the LLE about the stationary solution and finding all the eigenvalues of the linearized equation $\partial_\tau \delta\psi = \boldsymbol{\mathcal{L}}\delta\psi$ where $\delta\psi = (\delta\psi_r, \delta\psi_i)$ is the perturbation with real and imaginary parts $\delta\psi_{r,i}$, and

$$\boldsymbol{\mathcal{L}} = \begin{pmatrix} -1 - 2\psi_{st,r}\psi_{st,i} & \alpha - \psi_{st,r}^2 - 3\psi_{st,i}^2 + \frac{\beta}{2}\partial_\theta^2 \\ -\alpha + 3\psi_{st,r}^2 + \psi_{st,i}^2 - \frac{\beta}{2}\partial_\theta^2 & -1 + 2\psi_{st,r}\psi_{st,i} \end{pmatrix}. \qquad (2)$$

The eigenvalue equation $\boldsymbol{\mathcal{L}}\delta\psi = \lambda\delta\psi$ is then used to investigate the stability of the roll patterns. In our computational procedure, we discretize the system by only keeping an even number N of modes in the spectral domain, that can be spanned as $\Psi_l = \frac{1}{2\pi}\int_{-\pi}^{\pi} \psi(\theta)\, e^{-il\theta} d\theta$ with $l = -N/2, \ldots, N/2 - 1$. For the results reported here, we use $N = 512$ or $N = 1024$. We consistently evaluate the second derivative of θ in the wavenumber domain and the nonlinear terms in the θ-domain. Given a good initial guess for a stationary solution, we use the Levenberg-Marquardt algorithm to find the stationary solution. When finding the eigenvalues, the vector $\delta\psi$ of the eigenvalue equation becomes a column vector of length $2N$ after modal expansion. We use a spectral decomposition of the operator ∂_θ^2, which produces dense sub-blocks in the matrix representation of $\boldsymbol{\mathcal{L}}$ [11, 12]. We then use the QR algorithm to find all the eigenvalues. We have found that the spectral method adds negligibly to the computer time that we need for our implementations while reducing the angular resolution needed and enabling a direct comparison to our evolutionary studies, based on the split-step Fourier method. We use the boundary-tracking algorithm, described by Wang *et al.* [12], to find the stable operating region for the primary combs. We separately find the stable region for each primary comb of order L, whose comb spacing equals $L \times$ FSR, with L being a positive integer. We fix $\beta = -2.2 \times 10^{-3}$ through-

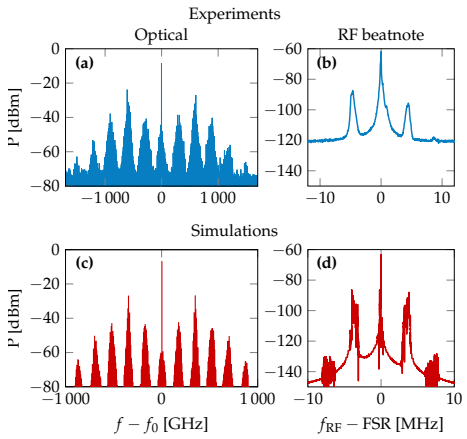

Fig. 3. (a) and (b) Combs and radio-frequency beatnotes obtained in a MgF_2 polished resonator in the vicinity of the spatiotemporal instability. (c) and (d) Comb and RF spectra from the numerical simulation of the LLE with $F^2 = 12$ and $\alpha = -1$, providing a good agreement with the experimental results.

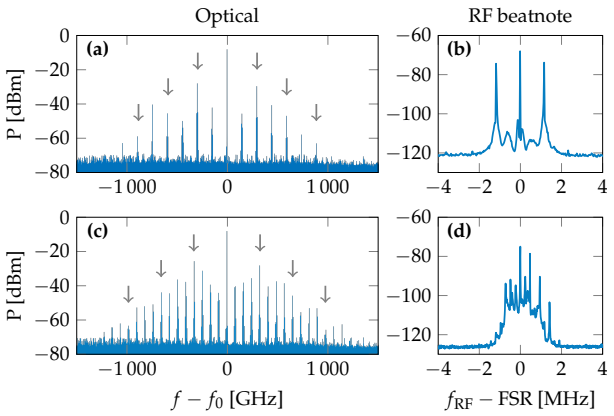

Fig. 4. Experimental results showing secondary and fourth-order combs in a MgF_2 WGM resonator. The combs are on the left column, and their corresponding photodetected beatnotes (around the fundamental frequency FSR = 5.9 GHz) are on right column. The arrows in the combs indicate the lines of the primary comb, before the spatiotemporal bifurcations.

out the letter, which corresponds to our experiments, and find the stable regimes in the two-dimensional α–F^2 parameter space. To find a stable region for a given value of L, we first find a solution in a highly stable region of the parameter space. We can then determine the stationary solution and its stability as the parameters vary. At some point, the stable solution becomes unstable or ceases to exist. We then move along or track the boundary, as described in ref. [12]. We note that different bifurcations occur at different points along the boundary, which is why it is important to determine all the eigenvalues. As a consequence, we observe cusps in the boundary of the stable region. In the laser frequency-power (or α–F^2) parameter space, Turing rolls with given multiplicity L have defined basins of attraction that can be thereby determined numerically.

The spatiotemporal perturbation has a specific signature in both the optical and radiofrequency domains. Indeed, in the optical domain, the stationary L-th order roll pattern can be expanded as $\psi_{st}(\theta) = \sum_k \Psi_{kL}\, e^{ikL\theta}$, with all the Ψ_{kL} being evidently constant. When a spatiotemporal bifurcation occurs, the amplitude of this pattern is perturbed following $\psi_{mod}(\theta,\tau) = [1 + a(\theta,\tau)]\,\psi_{st}(\theta)$, with the traveling-wave perturbation $a(\theta,\tau) = a_0\, e^{i(L_a\theta - \Omega_a\tau)}$. In the particular case when $L_a = L/2$, we have obtain the so-called secondary combs and the resulting pattern can be expanded as

$$\psi_{mod}(\theta,\tau) = \sum_k \Psi_{kL}\, e^{ikL\theta} + a_0\, e^{-i\Omega_a\tau} \sum_k \Psi_{kL}\, e^{iL\left(k+\frac{1}{2}\right)\theta}, \qquad (3)$$

where the first term in the right-hand side stands for the unperturbed pattern ψ_{st}, while the second term stands for the time-dependent, frequency-shifted comb lines created by the spatiotemporal perturbation. Note that the new spectral components of the secondary comb are located in-between those of the initial primary comb.

Figure 2 presents a detailed analysis of the spatiotemporal bifurcation as the laser detuning is varied. The leftmost column shows how, from an initial primary comb with multiplicity $L = 64$, the secondary comb first emerges and then gradually grows towards a fully chaotic comb. The second column displays numerical simulations that are in excellent agreement with the experimental spectra. It is interesting to note here the LLE is capable to match the experimental data over a very large dynamical range (80 dB) and for a high-dimensional system (there are $\sim$ 400 oscillating modes in these spectra). The numerical simulations presented in the third column unveil the dynamics of the rolls as they undergo the spatiotemporal bifurcation. Initially, the roll pattern is stationary, but after the bifurcation, it starts to oscillate both in space and time. This specific dynamics actually corresponds to the modulation of the intensity pattern by a traveling wave following $|\psi_{mod}(\theta,\tau)|^2 \simeq [1 + 2|a_0|\cos(L_a\theta - \Omega_a\tau)]|\psi_{st}(\theta)|^2$ for $|a_0| \ll 1$. Since $L_a \equiv L/2$, the effect of the instability-induced traveling wave δa is to trigger antiphase oscillations for adjacent rolls. As the system is driven further from the bifurcation, the pattern enters a regime of spatiotemporal chaos where the rolls are destroyed. The fourth and last column of Fig. 2 displays the eigenvalue distribution for the cavity modes. It can be seen that the bifurcation occurs when two of these eigenvalues cross the imaginary axis. The crossing of additional pairs of eigenvalue drives the intracavity field into a regime of spatiotemporal optical turbulence.

The spectral signature of the spatial bifurcation can be monitored in the optical spectrum, but the time-averaging of Fourier spectra does not allow the direct detection of the temporal dynamics for these modes. Instead, the temporal bifurcation can be analyzed via the emergence of modulation side peaks in the photodetected RF spectra of the combs. The comparison between theoretical and experimental results is performed via the output optical signal $\psi_{out} = -F + 2\rho\,\psi$ where ρ is the ratio between out-coupling and total losses. After photodetection, a radio-frequency signal proportional to the incoming optical power $|\psi_{out}|^2$ is generated, and features a multi-harmonic signal, and would feature spectral components of frequency $n \times \Omega_{FSR}$, with $n = 0, 1, 2, \ldots$. The photodetected optical power can be Fourier-expanded as

$$|\psi_{out}|^2 = \frac{1}{2}\mathcal{M}_0 + \sum_{n=1}^{+\infty}\left[\frac{1}{2}\mathcal{M}_n\, \exp(in\Omega_{FSR}t) + \text{c.c.}\right], \qquad (4)$$

where $\mathcal{M}_n = 2\sum_l \Psi_{out,l+n}\,\Psi^*_{out,l}$ is the slowly-varying envelope of the microwave spectral component of frequency $n \times \Omega_{FSR}$,

and c.c. stands for the complex conjugate of the preceding terms. We therefore expect the temporal bifurcation to induce modulation sidepeaks around $\mathcal{M}_n$, with a spectral spread that is of the order of WGM resonance linewidths (few MHz). This behavior is experimentally observed in Fig. 3, in agreement with our numerical simulations. It is important to note that these modulation side peaks are interaction with the main modes via four-wave mixing, thereby creating sub-combs that play a major role in phase-locking phenomena across the comb [13–15]. Indeed, as the system evolves further from the spatiotemporal bifurcation, the secondary combs in Fig. 2 feature several lines that are created around the initial bifurcation-induced modes. These parasitic lines, spaced by one FSR, are strengthened and amplified by four-wave mixing. They are useful experimentally because without them, we would not be able to photodetect a beatnotes around the FSR [since the "fundamental" tone would be $(L/2) \times \mathrm{FSR} \sim 150$ GHz away, that is, way above the bandwidth of the photodetector].

Interestingly, the spatiotemporal bifurcation can lead to higher-order bifurcation patterns, as displayed in Fig. 4. Effectively, we observe experimentally that the roll patterns can loose their stability to a secondary patterns, but can as well bifurcate towards a fourth-order pattern where $L_a \simeq L/4$: in that case, there are three (groups of) instability-induced lines in between the primary comb teeth, instead of just one as generally observed in secondary comb. The beatnote spectrum features a series of sharp modulation peaks that indicate that this new spatiotemporal pattern oscillates following a well-defined set of modulation frequencies.

In conclusion, we have shown that rolls can loose their stability via a spatiotemporal bifurcation that leads to simultaneous oscillations in space and time, via a traveling-wave amplitude modulation. The resulting pattern can lead to the well-known secondary combs, but we have also provided evidence, for the first time, of the existence of fourth-order combs. We expect these results to allow for a deeper understanding of the dynamics of many other dissipative structures in WGM resonators [16, 17], and permit as well to optimize the stability of these patterns for the many targeted applications [18–22].

FUNDING INFORMATION

ERC projects StG NextPhase (278616) and PoC Versyt (632108); CNES Project SHYRO.

REFERENCES

1. L. W. Liou, X. D. Cao, C. J. McKinstrie and G. P. Agrawal, "Spatiotemporal instabilities in dispersive nonlinear media," Phys. Rev. A **46**, 4202 (1992).
2. M. Anderson, F. Leo, S. Coen, M. Erkintalo, and S. G. Murdoch, "Observations of spatiotemporal instabilities of temporal cavity solitons," Optica **3**, 1071 (2016).
3. A. B. Matsko, A. A. Savchenkov, W Liang, V. S. Ilchenko, D. Seidel, and L. Maleki "Mode-locked Kerr frequency combs," Opt. Lett. **36**, 2845 (2011).
4. Y. K. Chembo and C. R. Menyuk, "Spatiotemporal Lugiato-Lefever Formalism for Kerr- Comb Generation in Whispering-Gallery-Mode Resonators," Phys. Rev. A **87**, 053852 (2013).
5. S. Coen, H. G. Randle, T. Sylvestre, and M. Erkintalo, "Modeling of octave-spanning Kerr frequency combs using a generalized mean-field Lugiato-Lefever model," Opt. Lett. **38**, 37 (2013).
6. G. Lin and Y. K. Chembo, "Phase-locking transition in Raman combs generated with whispering gallery mode resonators," Opt. Lett. **41**, 3718 (2016).
7. G. Lin, S. Diallo, J. Dudley and Y. K. Chembo, "Universal nonlinear scattering in ultra-high Q whispering gallery-mode resonators," Opt. Express **24**, 14880 (2016).
8. C. Godey, I. V. Balakireva, A. Coillet, and Y. K. Chembo, "Stability analysis of the spatiotemporal Lugiato-Lefever model for Kerr optical frequency combs in the anomalous and normal dispersion regimes," Phys. Rev. A **89**, 063814 (2014).
9. P. Parra-Rivas, D. Gomila, M. A. Matías, S. Coen, and L. Gelens, "Dynamics of localized and patterned structures in the Lugiato-Lefever equation determine the stability and shape of optical frequency combs," Phys. Rev. A **89**, 043813 (2014).
10. L. Delcey and M. Haragus, "Periodic waves of the Lugiato–Lefever equation at the onset of Turing instability," Phil. Trans. R. Soc. A **376**, 20170188 (2018).
11. J. A. C. Weideman and S. C. Reddy, "A MATLAB Differentiation Suite," ACM Trans. Math. Software **26**, 465 (2000).
12. S. Wang, A. Docherty, B. S. Marks, and C. R. Menyuk, "Boundary Tracking Algorithms for Determining the Stability of Mode-Locked Pulses," J. Opt. Soc. Am. B **31**, 2914 (2014).
13. T. Herr, K. Hartinger, J. Riemensberger, C. Y. Wang, E. Gavartin, R. Holzwarth, M. L. Gorodetsky and T. J. Kippenberg, "Universal formation dynamics and noise of Kerr-frequency combs in microresonators," Nature Photon. **6**, 480 (2012).
14. J. Li, H. Lee, T. Chen, and K. J. Vahala, "Low-Pump-Power, Low-Phase-Noise, and Microwave to Millimeter-Wave Repetition Rate Operation in Microcombs," Phys. Rev. Lett. **109**, 233901 (2012).
15. P. Del'Haye, K. Beha, S. B. Papp, and S. A. Diddams, "Self-Injection Locking and Phase-Locked States in Microresonator-Based Optical Frequency Combs," Phys. Rev. Lett. **112**, 043905 (2014).
16. D. C. Cole, E. S. Lamb, P. Del'Haye, S. A. Diddams and S. B. Papp, "Soliton crystals in Kerr resonators," Nat. Photon. **11**, 671 (2017).
17. A. Fulop, M. Mazur, A. Lorences-Riesgo, O. Helgason, P.-H. Wang, Y. Xuan, D. Leaird, M. Qi, P. Andrekson, A. Weiner, and V. Torres-Company, "High-order coherent communications using mode-locked dark-pulse Kerr combs from microresonators," Nature Commun. **9**, 1598 (2018).
18. T. J. Kippenberg, R. Holzwarth, and S. A. Diddams, "Microresonator-based optical frequency combs," Science **332**, 555-559 (2011).
19. Y. K. Chembo, "Kerr optical frequency combs: theory, applications and perspectives," Nanophotonics, **5**, 214 (2016).
20. G. Lin, A. Coillet and Y. K. Chembo, "Nonlinear photonics with high-Q whispering-gallery-mode resonators," Adv. Opt. Phot. **9**, 828 (2017).
21. A. Pasquazi, M. Peccianti, L. Razzari, D. Moss, S. Coen, M. Erkintalo, Y. K. Chembo, T. Hansson, S. Wabnitz, P. Del'Haye, X. Xue, A. M. Weiner, and R. Morandotti, "Micro-combs: A novel generation of optical sources," Phys. Rep. **729**, 1 (2018).
22. B. Stern, X. Ji, Y. Okawachi, A. L. Gaeta and M. Lipson, "Battery-operated integrated frequency comb generator," Nature **562**, 401 (2018).